

Effects of Self-Hybridized Exciton-Polaritons on TMDC Photovoltaics

Adam D. Alfieri, Tobia Ruth, Cheryl Lim, Jason Lynch, and Deep Jariwala*



Cite This: *Nano Lett.* 2025, 25, 3020–3026



Read Online

ACCESS |



Metrics & More



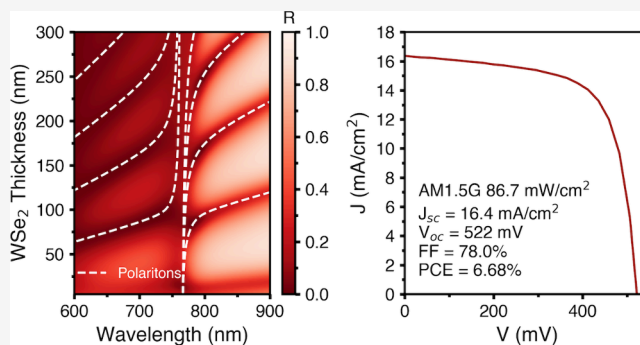
Article Recommendations



Supporting Information

ABSTRACT: Hybrid light-matter states called exciton-polaritons have been explored to improve excitonic photovoltaic (PV) and photodiode efficiency, but the use of closed cavity structures results in efficiency gains over a narrow band, with losses in the short circuit current density under solar illumination. In WX_2 ($X = S, Se$), the simultaneous large optical constants and strong exciton resonance can result in self-hybridized exciton-polaritons (SHEPs) emerging from the strong coupling of excitons and optical cavity modes formed by WX_2 . We perform thickness dependent device characterization of WS_2 and WSe_2 PVs to show that self-hybridized strong coupling enhances device efficiency on resonance while still enabling broadband absorption, resulting in improved short circuit current density under solar illumination. Ultimately, we leverage strong coupling to achieve external quantum efficiencies as high as 70% and record power conversion efficiencies approaching 7%. This result indicates the utility of SHEPs for light-energy harvesting applications.

KEYWORDS: Photovoltaics, Exciton-polaritons, Optoelectronics, Transition metal dichalcogenides, Quantum efficiency



Exciton-polaritons (EPs) are part-light, part-matter hybrid states arising from the strong coupling (SC) of excitons and photons in an optical cavity, typically a Fabry–Perot (FP) cavity.^{1–3} While EPs are typically studied for light emission applications, the low effective mass,⁴ long-range energy transfer,^{5–9} and strong absorption of polaritons makes them attractive for light harvesting.

Previous studies of EP light harvesting devices have been performed using organic semiconductors as the excitonic material inserted in a FP cavity consisting of a nearly perfectly reflecting bottom mirror and a partially transparent top mirror. These works have demonstrated that SC can enhance external quantum efficiency (EQE) of PVs at resonant conditions, with some evidence that SC can enhance the internal quantum efficiency (IQE).^{10,11} However, the closed cavity results in an overall decrease in the short circuit current density under broadband illumination, making these systems unsuitable for solar-energy harvesting.

Alternatively, films with simultaneously strong exciton resonances and sufficiently high refractive index can form self-hybridized exciton-polaritons (SHEPs) in open cavity systems.^{12–14} SHEPs are less useful for light emission due to lower cavity quality factors than closed cavity systems, but the same broad line widths make these systems interesting for energy harvesting. Using a self-hybridized system enables off-resonance absorption in the active layer, improving the practicality of EP devices for energy harvesting.

Transition metal dichalcogenides (TMDCs) are van der Waals (vdW) materials that exhibit strong interaction with

light due to large exciton oscillator strengths, even in bulk form,^{15,16} and high refractive indices, enabling strong absorption in thin layers.^{17–20} Therefore, TMDCs have attracted significant attention as materials for next generation optoelectronics with thin, stable, and nontoxic active layers.^{21–26} SHEPs have been demonstrated in the disulfides and diselenides of Mo and W, with Rabi splitting values of approximately 200 meV.²⁷ Consequently, it is important to understand how SHEPs can affect optoelectronic devices, both for the design of TMDC PVs and more generally as a model system that can be extended to other high-index excitonic semiconductors, both known and to be discovered.

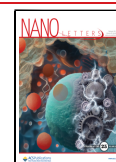
In this work, we consider WS_2 and WSe_2 as model systems in which we leverage both the large optical constants and excitonic properties to fabricate photovoltaics that exhibit SHEPs to understand how these states may be used for energy harvesting in high-index excitonic semiconductors. We fabricate >4 dozen devices from 10 to 300 nm in thickness to alter the cavity energy and cover the polariton dispersion. We show that the absorption through SHEPs can enable enhanced short circuit current densities and efficiencies in PVs

Received: January 18, 2025

Revised: February 4, 2025

Accepted: February 5, 2025

Published: February 7, 2025



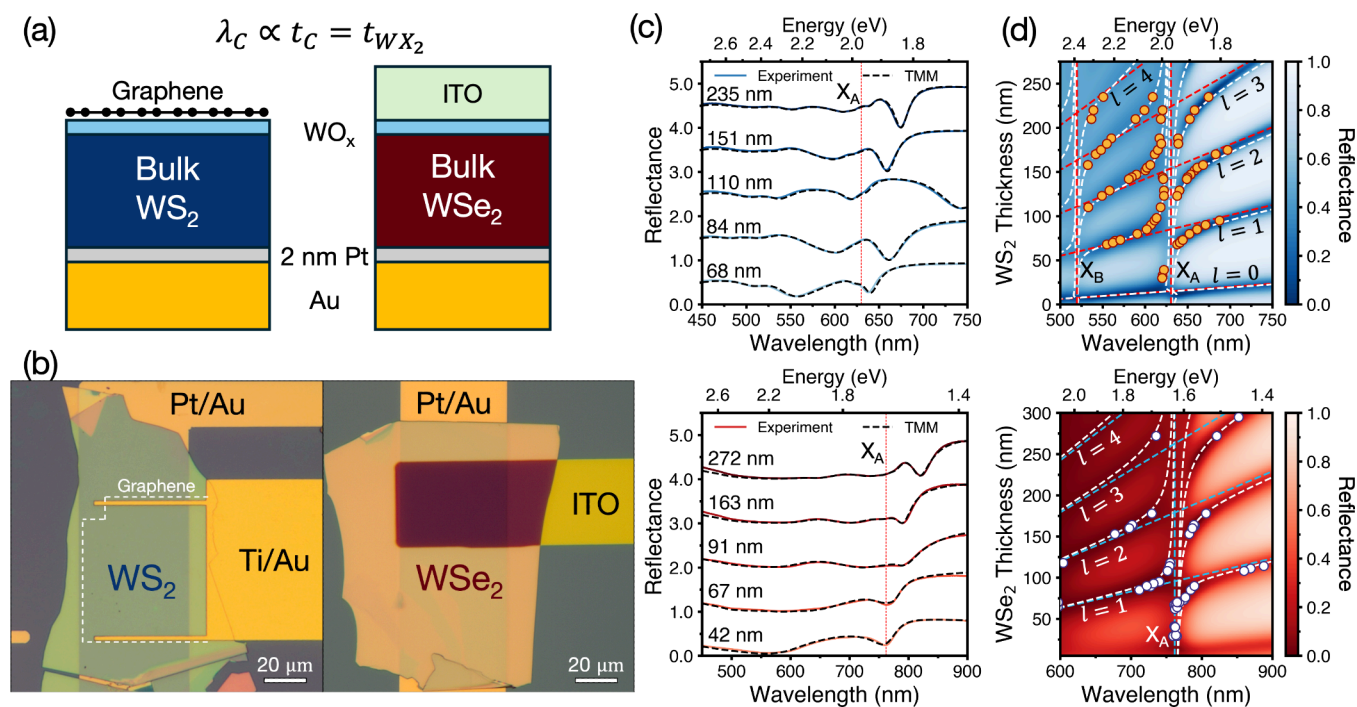


Figure 1. Device structures and exciton-polariton dispersions. (a) The structures of the SHEP PV devices from WS₂ (left) and WSe₂ (right). (b) Optical microscope images of representative WS₂ (left) and WSe₂ (right) devices. (c) Measured reflectance spectra (solid lines) and TMM calculated spectra (dashed lines) for various thicknesses of WS₂ (top) and WSe₂ (bottom) devices. Spectra are shifted vertically for clarity. The red dashed lines correspond to the A exciton. (d) TMM calculated reflectance as a function of thickness and wavelength for WS₂ (top) and WSe₂ (bottom) devices. Fits to the coupled oscillator model are overlaid as dashed white lines, while the diagonal and vertical, colored lines are the cavity modes and the exciton energies. The cavity mode orders and excitons are labeled. The minima in the reflectance spectra for samples of various thicknesses are overlaid as orange dots for WS₂ and white dots for WSe₂.

both on resonance and under solar illumination, opening new avenues in photovoltaic science and device engineering.

We fabricate PVs from mechanically exfoliated WS₂ and WSe₂ flakes using two different top electrode configurations (Figure 1a). The WS₂ devices use a transferred graphene layer with Ti/Au contacts. The WSe₂ devices have a ~67 nm In₂O₃:SnO₂ (ITO) top electrode instead of graphene; the ITO acts as both an electrode and an antireflective coating (ARC), similar to a previous report.²⁸ Due to the optical impedance contrast between the WSe₂ and ITO, the structure still supports FP cavity modes in the WSe₂. In both cases, we use 2 nm Pt/70 nm Au/5 nm Ti bottom electrodes and an electron selective WO_x top layer, based on a previous work²¹ (see Methods for details). The sharper exciton peak and lack of an ARC make the WS₂ devices better for studying the resonant response of the polariton modes. The ITO/WSe₂ devices offer a better system to leverage SHEPs for broadband light harvesting and improved device performance. Figure 1b shows representative devices. Laser beam induced current (LBIC) is used to determine the active area (Figure S4).

Figure 1c shows the experimentally measured and transfer matrix method²⁹ (TMM)-calculated reflectance spectra for devices with various thicknesses of WS₂ (top) and WSe₂ (bottom), showing the accuracy of TMM. Figure 1d shows the TMM-calculated reflectance as a function of photon energy and TMDC thickness to study the EP dispersion for WS₂ (top) and WSe₂ (bottom). Minima in measured reflectance spectra for representative devices are overlaid as dots, showing excellent agreement between experiment and TMM calculation. The polariton modes are easily identified as sharp reflectance minima featuring an anticrossing between the cavity

mode and exciton energy. The polariton modes are fit as the eigenvalues of the multimode, multiexciton coupled oscillator Hamiltonian for a system with *l* FP cavity modes and *m* exciton states (Methods).^{30,31} The energies of the FP cavity modes generally depend on thickness and incident angle. However, the massive optical impedance of WX₂ results in negligible dispersion with incident angle (Figure S3). Therefore, all measurements are conducted at normal incidence, and the cavity energy is tuned only by the WX₂ thickness.

In addition to the $\sim l\lambda/(2n)$ (with *l* an integer and *n* the refractive index) FP cavity modes, there is a deep subwavelength interference mode³² for thinner (<20 nm) WS₂ films that interacts with the exciton in the weak coupling regime, leading to a Fano resonance that causes the blue shifting of the reflectance minima from the bare exciton peaks for thicknesses below 50 nm.³³ We focus on the $\sim l\lambda/(2n)$ cavity modes where *l* is 1, 2, and 3, which all exhibit SC (Table S1), and we further limit our focus to the A exciton in each material as it has the largest oscillator strength, narrowest line width, and lowest energy. For the remainder of this work, we refer to the polariton branch at higher energies than the A exciton as the upper polariton (UP) and the polariton branch at lower energies as the lower polariton (LP). The Rabi splitting for the first 3 polariton modes of WS₂ are 195.8, 196.9, and 196.0 meV for WS₂ and 144.7, 172.3, and 178.6 meV for WSe₂, respectively. The lower Rabi splitting values for WSe₂ can be attributed to the slightly weaker oscillator strength and broader exciton transition.

We now investigate the effects of SHEPs on EQE and power conversion efficiency (PCE) of WS₂ devices as a function of wavelength. Figure 2a and 2b shows the EQE and PCE spectra

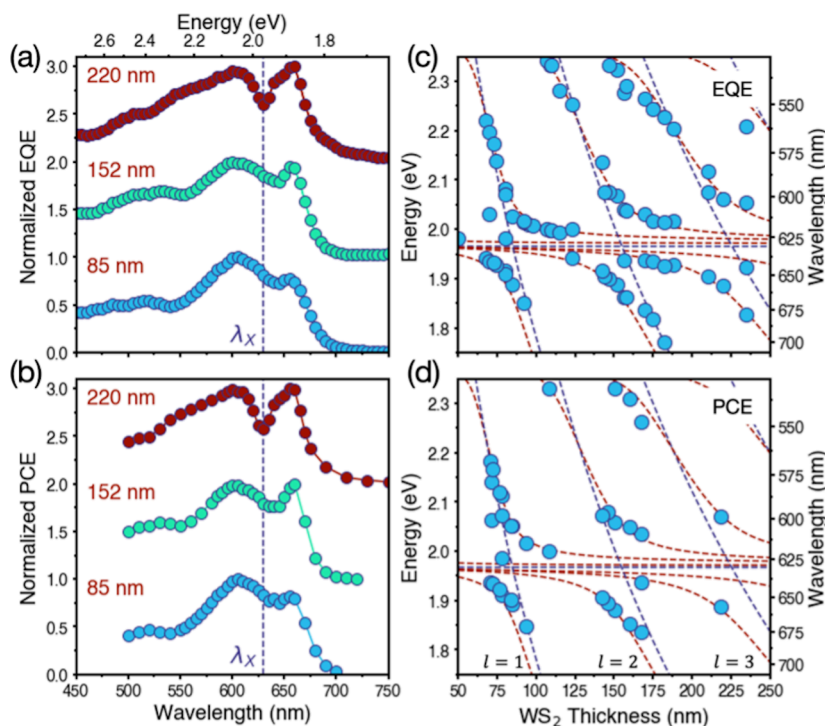


Figure 2. Spectral EQE and PCE. Self-normalized EQE (a) and monochromatic PCE (b) spectra for representative devices with WS₂ thicknesses of 85, 152, and 220 nm, corresponding to approximate zero-detuning thicknesses for polaritons arising from the first, second, and third order FP cavity modes, respectively. The spectra are shifted vertically for clarity. The wavelength corresponding to the bare exciton, λ_x , is denoted by the dark blue dashed line. Peaks in the EQE (c) and PCE (d) spectra as a function of WS₂ thickness overlaid on the polariton dispersions (red dashed lines) and the bare exciton and cavity energies (blue dashed lines).

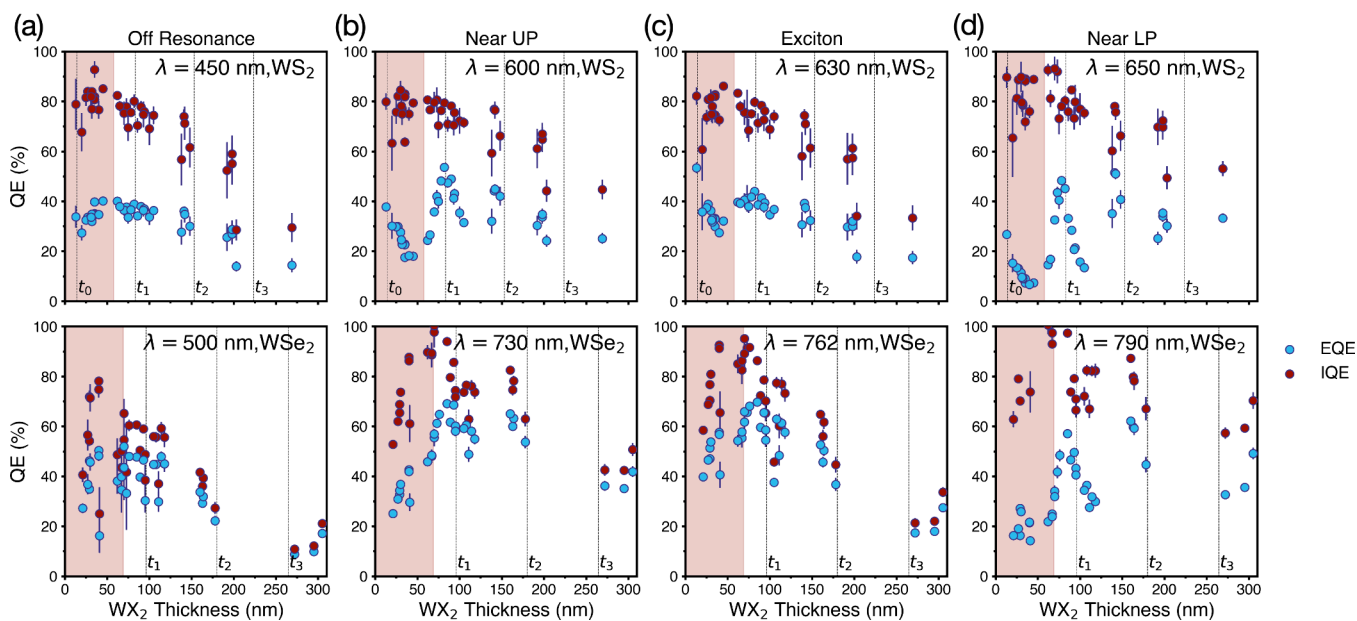


Figure 3. Thickness dependent EQE and IQE. External (blue) and internal (red) quantum efficiencies for WS₂ (top) and WSe₂ (bottom) determined by photocurrent mapping with a tunable laser at a wavelength that is (a) off resonance (450 nm for WS₂, 500 nm for WSe₂), (b) near the zero-detuning upper polariton (600 and 730 nm), (c) near the exciton (630 and 762 nm), and (d) near the zero-detuning lower polariton (650 and 790 nm). The weak coupling (WC) regime is denoted by red shading while the strong coupling (SC) regime is unshaded. The thicknesses, t_l ($l = 1, 2, 3$), corresponding to zero detuning of the $l = 1, 2, 3$ cavity modes are denoted with black dotted lines.

for representative devices near zero detuning, $\Delta_l(t) = E_C^{(l)}(t) - X_A$ (where $E_C^{(l)}(t)$ is the energy of cavity mode l and X_A is the energy of the A exciton), for the first 3 FP cavity mode polaritons (see Figure S5. for quantitative EQE and PCE values). Each EQE and PCE spectrum exhibits clear peaks

corresponding to the UP and LP resonances. This is clearly shown in Figure 2c and 2d, which plot the energies of the peaks for each EQE (Figure 2c) and PCE (Figure 2d) spectra as a function of thickness. The peaks are overlaid over the polariton dispersion and follow the dispersion of the polariton

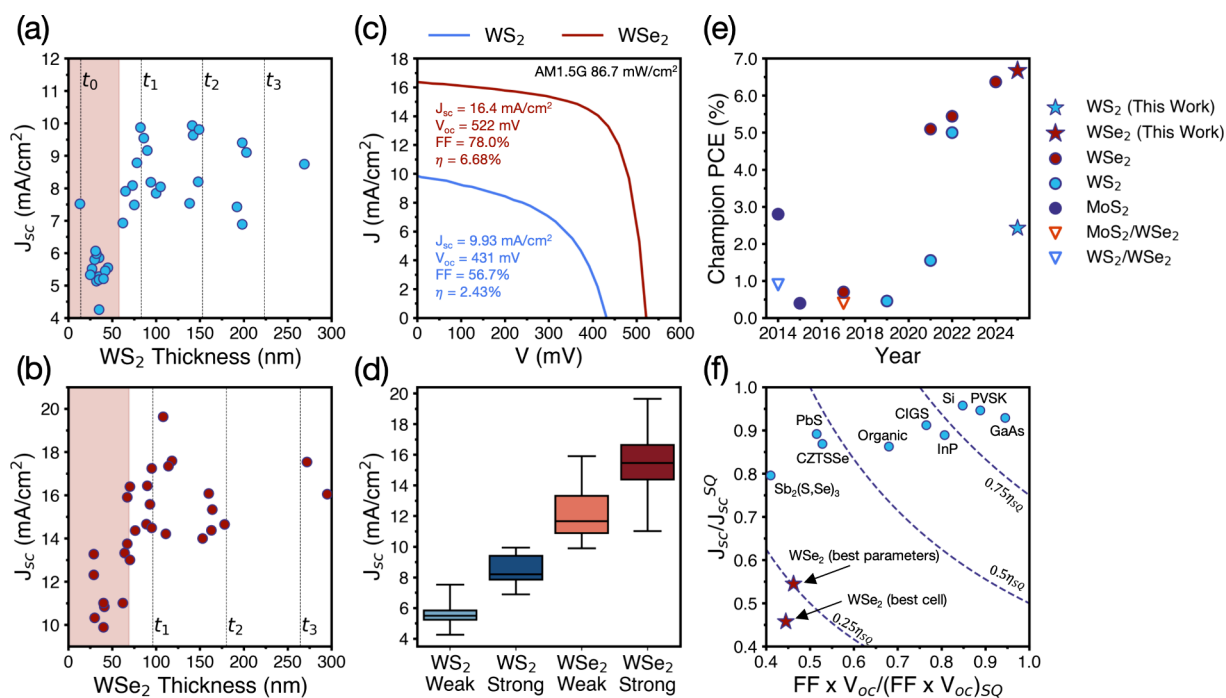


Figure 4. Photovoltaic performance. Short circuit current density (J_{sc}) under simulated AM1.5G irradiation as a function of thickness for (a) WS₂ and (b) WSe₂. The thicknesses, t_l ($l = 1, 2, 3$), corresponding to zero detuning of the $l = 1, 2, 3$ cavity modes are denoted by black dotted lines. The weak coupling regime is shaded in red. (c) J - V curves of champion devices from WS₂ and WSe₂. J_{sc} , V_{oc} , open circuit voltage (V_{oc}), fill factor (FF), and power conversion efficiency (η) are given for each device. (d) Boxplot of J_{sc} for devices grouped by material and coupling regime (strong or weak). (e) Reported TMDC photovoltaic efficiencies under AM1.5G illumination over time,^{21–23,28,37–41} see Table S2 for details. (f) Our best WSe₂ cell and the best J_{sc} , V_{oc} , and FF across all our devices compared with more mature technologies in terms of J_{sc} and the product of FF and V_{oc} normalized to the Shockley-Queisser (SQ) limited values for these parameters. Dashed lines correspond to 25%, 50%, and 75% of the SQ limited efficiency, η_{SQ} . All data points are taken as the highest confirmed values for single junction cells under AM1.5G illumination from ref 42 except for PbS, which is taken from ref 43. Perovskite is abbreviated to “PVSK”.

modes remarkably well, evidencing the beneficial effect of polariton states on photovoltaic performance. Multiple peaks can emerge in the spectra due to multiple polariton mode orders. The clear resemblance of PCE extracted from monochromatic I–V characteristics with polaritonic dispersion presents strong evidence of the effect of SHEPs directly on the PCE of WS₂ PVs. WSe₂ devices do not exhibit prominent peaks in the spectral EQE (Figure S6) due to strong off-resonant absorption and parasitic absorption on resonance (Figure S2), but the response is extended further into the IR, below the direct bandgap.

Understanding the thickness dependent device physics requires thickness dependent EQE and IQE at on and off-resonant conditions. Figure 3 shows the thickness dependent EQE (blue dots) and IQE (red dots) of WS₂ (top) and WSe₂ (bottom) devices as a function of thickness at 4 different wavelengths. WS₂ devices are characterized at wavelengths of 450 nm (off resonance), 600 nm (near UP when $\Delta = 0$), 630 nm (near bare exciton), and 650 nm (near LP when $\Delta = 0$). WSe₂ devices are characterized under 500, 730, 762, and 790 nm illumination, using the same criteria for choosing wavelengths. Dashed lines are included to indicate the thicknesses corresponding to $\Delta_l(t_l) = 0$ for the $l = 1, 2$, and 3 FP cavity modes, respectively. We denote the weak coupling (WC) regime with red shading. The cutoff is chosen to be at a point where the first cavity mode energy is detuned $4g$ above the exciton energy, resulting in an exciton fraction of approximately 95% for the LP. To eliminate uncertainty related to the active area, we use a focused, tunable laser beam

with a spot size of approximately $2 \mu\text{m}$ in diameter at 25 points on each device and extract the average and standard deviation of the short circuit current (Methods).

Due to the electric field enhancement of the polariton states, the electrode layers exhibit large parasitic absorption peaks (Figure S2). To study the IQE, we must only consider the absorption in the WX₂ active layers, which must be extracted from layer-resolved absorption with the transfer matrix model (Figure S2). The IQE is simply the EQE normalized by the active layer absorption, decoupling effects of collection efficiency from absorption.

$$\text{IQE}(\lambda) = \frac{\text{EQE}(\lambda)}{A_{\text{active}}(\lambda)}$$

For WS₂ devices (Figure 3a), peaks in the EQE emerge near the t_1 and t_2 condition for the 600 and 650 nm illuminations, clearly demonstrating resonant enhancement in efficiency due to the UP and LP. For the LP, the efficiency enhancement is by a factor of nearly 10. Importantly, the high IQE values near the resonant condition indicate that the SHEPs can be efficiently converted to photocurrent. The IQE begins to decrease with thickness beyond approximately 100 nm in the WS₂ devices, which is well-predicted by free carrier drift-diffusion (DD) modeling that assumes a low (0.01 – $0.1 \text{ cm}^2/(\text{V s})$) carrier mobility for out-of-plane transport (Figure S13).

WSe₂ devices (Figure 3b) exhibit similar enhancement in the EQE near t_1 and t_2 under illumination by 730 and 790 nm light. However, the EQE enhancement is not as drastic compared to WS₂ due to the ITO ARC, which results in more

off-resonant absorption. In WSe_2 , the primary benefit of strong coupling can therefore be thought of as extending the absorption below the optical bandgap, with some additional resonant enhancement at the UP and near the exciton due to large line widths and higher order modes.

The results for the WSe_2 EQE and IQE are predicted by DD calculations except for decreased QE at low thicknesses. The deviation at lower thicknesses and poorer IQE at short wavelength illumination suggests that the sputtered ITO/ WO_x contact may have more defects than the transferred G/ WO_x contact. We therefore attribute the slight IQE drop for thinner WSe_2 devices to recombination near the front contact at trap sites induced by sputtering. Beyond 70–90 nm, bulk SRH recombination dominates, and the IQE drops. The IQE decrease for thicker devices is less severe for 730 and 790 nm illumination, with IQE of $\sim 70\%$ under 790 nm illumination for a device >300 nm in thickness. This effect is predicted by the DD model and is therefore expected to be related to the generation profile. The overall agreement with free carrier DD calculations suggests that, while the absorption is dominated by excitons and EPs, the transport is dominated by free carriers. This suggests facile ionization of excitons and EPs enabled by relatively low exciton binding energies.³⁴ The combination of strong excitonic/polaritonic absorption and free carrier transport is ideal for optoelectronics. Overall, the thickness dependent EQE/IQE results confirm the resonant enhancement of SHEPs in both device structures while elucidating the factors limiting charge collection.

Finally, we consider photovoltaic measurements under solar simulation conditions (Methods, Figure S8). Figure 4a and 4b shows J_{sc} under solar simulation as a function of thickness for WS_2 and WSe_2 devices. In both cases, J_{sc} increases as the thickness transitions to the SC regime: the first demonstration of broadband J_{sc} enhancement from EPs, which we emphasize is enabled by self-hybridization. This result is predicted by DD modeling (Figure S12). Figure 4d shows box plots of J_{sc} for WS_2 and WSe_2 in the SC and WC regimes, further demonstrating the enhancement in J_{sc} enabled by SHEPs for both device structures. The WSe_2 devices have a larger J_{sc} than the WS_2 devices for all thicknesses due to the smaller bandgap and ARC. Interestingly, the J_{sc} in the WS_2 devices increases at ultrathin thicknesses close to the t_0 Fano resonance, and the WS_2 device at ~ 13 nm thickness exhibits a J_{sc} comparable to devices in the SC regime and larger than devices in the WC regime between t_0 and t_1 , indicating the potential for extremely thin absorber PVs leveraging the broadband interference effect.¹⁹

While the J_{sc} reaches a maximum near the t_1 condition, the optimal thickness for charge collection occurs at smaller thicknesses for both WS_2 and WSe_2 . This is apparent in the IQE (Figure 3) and the FF (Figure S9), which both appear to decrease with thicknesses beyond approximately 70–80 nm. Therefore, there is a trade-off between absorption and charge collection. The WSe_2 devices tended to have better fill factor (FF) and V_{oc} than the WS_2 , with FF as high as 78%, and V_{oc} approaching 550 mV, which we expect is due to better transport and band alignment.

Figure 4c shows the light and dark curves of the best devices of each kind. The champion WS_2 /graphene device, with a thickness near the t_2 condition, exhibits a PCE of 2.43%. Leveraging the extended absorption and improved antireflective properties of the WSe_2 /ITO devices, we achieve a champion efficiency of 6.68% in a device with a thickness of 70

nm: slightly detuned from the t_1 condition and in the regime with optimal charge collection. The PCE is generally improved in the WSe_2 devices 70 nm and thicker (Figure S9). Figure 4e benchmarks our devices against past works. The 2.43% efficiency WS_2 device is among the most efficient WS_2 devices to date, while the 6.68% PCE WSe_2 device is the most efficient TMDC PV device reported in general. Importantly, we note that polaritonic effects, although not identified, were almost certainly present in previous works due to the similarity of the structures. Therefore, the absolute efficiency values reported here are of less importance than identifying SHEPs as an important light harvesting mechanism in TMDC PVs and other high-index excitonic semiconductors.

Contact variability in both the WS_2 /Graphene and WSe_2 /ITO devices makes it difficult to draw direct conclusions regarding relationships between SC and V_{oc} or IQE in these devices. We expect the V_{oc} to be invariable with thickness except for a decrease in V_{oc} below a critical thickness (Figure S12). The WSe_2 devices show no relationship between thickness and V_{oc} (Figure S9), but the WS_2 devices exhibit significant batch-to-batch variation of V_{oc} (Figure S10). Drift diffusion simulations further predict that the optimal thickness for PCE occurs at t_1 for both device structures despite the drop in FF with thickness. Given our results for J_{sc} and the agreement between experiment and DD results, we can therefore expect that SHEPs have an overall beneficial effect on the PCE of TMDC solar cells.

The WSe_2 solar cells here have significant room for improvement with respect to the Shockley-Queisser (SQ) limit.³⁵ In particular, J_{sc} and V_{oc} are far lower than the SQ limited values of 35.82 mA/cm² and 1.028 V for a 1.3 eV bandgap material.³⁶ Figure 4f shows J_{sc}/J_{sc}^{SQ} and $\text{FF} \times V_{oc}/(\text{FF} \times V_{oc})^{SQ}$ of our devices compared to those of more mature technologies. Significant improvement in both light and carrier management clearly will be necessary for TMDCs to be candidates as solar cell absorber materials. J_{sc} can be improved by reducing the optical loss of the ITO electrode and replacing the lossy Pt/Au bottom electrode with a thin hole transport layer and a low loss Ag back contact. Engineering V_{oc} will require contact optimization and identifying a suitable n-type heterojunction partner for WSe_2 with minimal conduction band offset. However, scaling TMDC solar cells beyond flake scale devices is a prerequisite that must be achieved before TMDCs can be considered as anything more than a model system to study optical and device physics.

In conclusion, our work presents self-hybridized exciton-polariton photovoltaics using bulk tungsten dichalcogenides as both the cavity and active excitonic material: the first demonstration of self-hybridized exciton-polariton optoelectronic devices. We demonstrate that exciton-polaritons can enhance absorption and be efficiently converted to current, benefiting both the external quantum efficiency and power conversion efficiency of photovoltaics. We show that self-hybridization enables enhancement of short circuit current density under broadband solar illumination in addition to efficiency enhancement on resonance. We balance enhanced absorption and efficient charge collection to achieve a WSe_2 photovoltaic with a record power conversion efficiency of $\sim 6.7\%$. These results elucidate the effects of thickness on TMDC PVs and, more generally, indicate that self-hybridized exciton-polaritons in high-index inorganic excitonic semiconductors are useful for solar photovoltaics and other forms of optical energy transduction.

■ ASSOCIATED CONTENT

Data Availability Statement

Data, materials, and code are available from the corresponding author upon reasonable request.

SI Supporting Information

The Supporting Information is available free of charge at <https://pubs.acs.org/doi/10.1021/acs.nanolett.5c00399>.

Methods, determination of electrode refractive indices, layer resolved absorption, calculated angle dependent reflectance, LBIC and active area calculation, quantitative spectral EQE and PCE, WSe₂ spectral response, experimental setup for EQE mapping measurements, solar simulation *J*–*V* curves, PV parameter statistics, batch dependent *V*_{oc} in WS₂ devices, spectral irradiance from solar simulator, drift diffusion modeling of PV characteristics, drift diffusion modeling of quantum efficiency, coupled oscillator model fit results, tabulated values and references for Figure 4d, parameters used in drift-diffusion simulations (PDF)

■ AUTHOR INFORMATION

Corresponding Author

Deep Jariwala – Department of Electrical and Systems Engineering, University of Pennsylvania, Philadelphia, Pennsylvania 19104, United States; orcid.org/0000-0002-3570-8768; Email: dmj@seas.upenn.edu

Authors

Adam D. Alfieri – Department of Electrical and Systems Engineering, University of Pennsylvania, Philadelphia, Pennsylvania 19104, United States

Tobia Ruth – Department of Electrical and Systems Engineering, University of Pennsylvania, Philadelphia, Pennsylvania 19104, United States

Cheryl Lim – Department of Electrical and Systems Engineering, University of Pennsylvania, Philadelphia, Pennsylvania 19104, United States

Jason Lynch – Department of Electrical and Systems Engineering, University of Pennsylvania, Philadelphia, Pennsylvania 19104, United States

Complete contact information is available at:

<https://pubs.acs.org/doi/10.1021/acs.nanolett.5c00399>

Author Contributions

D.J. conceived, supervised, and acquired funding for the project. A.D.A. and D.J. designed the experiments. A.D.A. fabricated the devices with assistance from T.R. and C.L. A.D.A., T.R., and C.L. performed the optoelectronic measurements. A.D.A. conducted the ellipsometry measurements and fit the data. J.L. fit preliminary ellipsometry data. A.D.A. performed the theoretical calculations, simulations, data processing, and data visualization. A.D.A. wrote the manuscript with inputs from all authors. All authors discussed the results and revised the manuscript.

Notes

The authors declare no competing financial interest.

■ ACKNOWLEDGMENTS

D.J., A.D.A. and T.R. acknowledge primary support from the Vagelos Institute for Energy Science and Technology. A.D.A. and D.J. acknowledge partial support from the Office of Naval

Research (ONR) Young Investigator Award (YIP) (N00014-23-1-203) Metamaterials Program. D.J. and J.L. acknowledge partial support from the Asian Office of Aerospace Research and Development of the Air Force Office of Scientific Research (AFOSR) FA2386-20-1-4074. D.J. acknowledges partial support from the Alfred P. Sloan Foundation's Sloan Fellowship in Chemistry. C.L. acknowledges support from the University of Pennsylvania Center for Undergraduate Research Fellowships. This work was conducted in its majority at the Singh Center for Nanotechnology at the University of Pennsylvania, which is supported by the NSF National Nanotechnology Coordinated Infrastructure Program grant no. NNCI1542153. The authors gratefully acknowledge the use of facilities and instrumentation (G2V Pico solar simulator) supported by the Department of Materials Science and Engineering Departmental Laboratory at the University of Pennsylvania. A.D.A. thanks Zirun Han and Mahfujur Rahaman for helping with aspects of experimental setup and Bongjun Choi for providing the photomask.

■ REFERENCES

- (1) Hopfield, J. J. Theory of the Contribution of Excitons to the Complex Dielectric Constant of Crystals. *Phys. Rev.* **1958**, *112* (5), 1555–1567.
- (2) Anantharaman, S. B.; Jo, K.; Jariwala, D. Exciton–Photonics: From Fundamental Science to Applications. *ACS Nano* **2021**, *15*, 12628–12654.
- (3) Gibbs, H. M.; Khitrova, G.; Koch, S. W. Exciton-Polariton Light-Semiconductor Coupling Effects. *Nat. Photonics* **2011**, *5* (5), 273.
- (4) Deng, H.; Haug, H.; Yamamoto, Y. Exciton-Polariton Bose–Einstein Condensation. *Rev. Mod. Phys.* **2010**, *82* (2), 1489–1537.
- (5) Steger, M.; Liu, G.; Nelsen, B.; Gautham, C.; Snoko, D. W.; Balili, R.; Pfeiffer, L.; West, K. Long-Range Ballistic Motion and Coherent Flow of Long-Lifetime Polaritons. *Phys. Rev. B - Condens. Matter Mater. Phys.* **2013**, *88* (23), 15–18.
- (6) Liu, B.; Lynch, J.; Zhao, H.; Conran, B. R.; McAleese, C.; Jariwala, D.; Forrest, S. R. Long-Range Propagation of Exciton-Polaritons in Large-Area 2D Semiconductor Monolayers. *ACS Nano* **2023**, *17* (15), 14442–14448.
- (7) Zhong, X.; Chervy, T.; Zhang, L.; Thomas, A.; George, J.; Genet, C.; Hutchison, J. A.; Ebbesen, T. W. Energy Transfer between Spatially Separated Entangled Molecules. *Angew. Chemie - Int. Ed.* **2017**, *56* (31), 9034–9038.
- (8) Zhong, X.; Chervy, T.; Wang, S.; George, J.; Thomas, A.; Hutchison, J. A.; Devaux, E.; Genet, C.; Ebbesen, T. W. Non-Radiative Energy Transfer Mediated by Hybrid Light-Matter States. *Angew. Chem.* **2016**, *128* (21), 6310–6314.
- (9) Son, M.; Armstrong, Z. T.; Allen, R. T.; Dhavamani, A.; Arnold, M. S.; Zanni, M. T. Energy Cascades in Donor-Acceptor Exciton-Polaritons Observed by Ultrafast Two-Dimensional White-Light Spectroscopy. *Nat. Commun.* **2022**, *13*, 7305.
- (10) Eizner, E.; Brodeur, J.; Barachati, F.; Sridharan, A.; Kéna-Cohen, S. Organic Photodiodes with an Extended Responsivity Using Ultrastrong Light-Matter Coupling. *ACS Photonics* **2018**, *5* (7), 2921–2927.
- (11) de Jong, L. M. A.; Berghuis, A. M.; Abdelkhalik, M. S.; van der Pol, T. P. A.; Wienk, M. M.; Janssen, R. A. J.; Rivas, J. G. Enhancement of the Internal Quantum Efficiency in Strongly Coupled P3HT-C60 Organic Photovoltaic Cells Using Fabry-Perot Cavities with Varied Cavity Confinement. *Nanophotonics* **2024**, *13*, 1–10.
- (12) Choi, B.; Jo, K.; Rahaman, M.; Alfieri, A.; Lynch, J.; Pribil, G. K.; Koh, H.; Stach, E. A.; Jariwala, D. Giant Optical Anisotropy in 2D Metal-Organic Chalcogenates. *ACS Nano* **2024**, *18*, 25489.
- (13) Anantharaman, S. B.; Stevens, C. E.; Lynch, J.; Song, B.; Hou, J.; Zhang, H.; Jo, K.; Kumar, P.; Blancon, J. C.; Mohite, A. D.;

- Hendrickson, J. R.; Jariwala, D. Self-Hybridized Polaritonic Emission from Layered Perovskites. *Nano Lett.* **2021**, *21* (14), 6245–6252.
- (14) Anantharaman, S. B.; Lynch, J.; Stevens, C. E.; Munley, C.; Li, C.; Hou, J.; Zhang, H.; Torma, A.; Darlington, T.; Coen, F.; Li, K.; Majumdar, A.; Schuck, P. J.; Mohite, A.; Harutyunyan, H.; Hendrickson, J. R.; Jariwala, D. Dynamics of Self-Hybridized Exciton–Polaritons in 2D Halide Perovskites. *Light Sci. Appl.* **2024**, *13* (1), 1.
- (15) Zhang, H.; Abhiraman, B.; Zhang, Q.; Miao, J.; Jo, K.; Roccasecca, S.; Knight, M. W.; Davoyan, A. R.; Jariwala, D. Hybrid Exciton–Plasmon–Polaritons in van Der Waals Semiconductor Gratings. *Nat. Commun.* **2020**, *11* (1), 3552.
- (16) Munkhbat, B.; Wrobel, P.; Antosiewicz, T. J.; Shegai, T. O. Optical Constants of Several Multilayer Transition Metal Dichalcogenides Measured by Spectroscopic Ellipsometry in the 300–1700 Nm Range: High Index, Anisotropy, and Hyperbolicity. *ACS Photonics* **2022**, *9*, 2398–2407.
- (17) Alfieri, A. D.; Motala, M. J.; Snure, M.; Lynch, J.; Kumar, P.; Zhang, H.; Post, S.; Bowen, T.; Muratore, C.; Robinson, J. A.; Hendrickson, J. R.; Glavin, N. R.; Jariwala, D. Ultrathin Broadband Metasurface Superabsorbers from a van Der Waals Semimetal. *Adv. Opt. Mater.* **2023**, *11* (4), 2202011.
- (18) Kumar, P.; Lynch, J.; Song, B.; Ling, H.; Barrera, F.; Kisslinger, K.; Zhang, H.; Anantharaman, S. B.; Digani, J.; Zhu, H.; Choudhury, T. H.; McAleese, C.; Wang, X.; Conran, B. R.; Whear, O.; Motala, M. J.; Snure, M.; Muratore, C.; Redwing, J. M.; Glavin, N. R.; Stach, E. A.; Davoyan, A. R.; Jariwala, D. Light–Matter Coupling in Large-Area van Der Waals Superlattices. *Nat. Nanotechnol.* **2022**, *17* (2), 182–189.
- (19) Jariwala, D.; Davoyan, A. R.; Tagliabue, G.; Sherrott, M. C.; Wong, J.; Atwater, H. A. Near-Unity Absorption in van Der Waals Semiconductors for Ultrathin Optoelectronics. *Nano Lett.* **2016**, *16* (9), 5482–5487.
- (20) Lin, D.; Lynch, J.; Wang, S.; Hu, Z.; Rai, R. K.; Zhang, H.; Chen, C.; Kumari, S.; Stach, E.; Davydov, A. V.; Redwing, J. M.; Jariwala, D. Broadband Light Harvesting from Scalable Two-Dimensional Semiconductor Heterostructures. *Nano Lett.* **2024**, *24*, 13935–13944.
- (21) Kim, K. H.; Andreev, M.; Choi, S.; Shim, J.; Ahn, H.; Lynch, J.; Lee, T.; Lee, J.; Nazif, K. N.; Kumar, A.; Kumar, P.; Choo, H.; Jariwala, D.; Saraswat, K. C.; Park, J. H. High-Efficiency WSe₂ Photovoltaic Devices with Electron-Selective Contacts. *ACS Nano* **2022**, *16* (6), 8827–8836.
- (22) Nassiri Nazif, K.; Daus, A.; Hong, J.; Lee, N.; Vaziri, S.; Kumar, A.; Nitta, F.; Chen, M. E.; Kananian, S.; Islam, R.; Kim, K. H.; Park, J. H.; Poon, A. S. Y.; Brongersma, M. L.; Pop, E.; Saraswat, K. C. High-Specific-Power Flexible Transition Metal Dichalcogenide Solar Cells. *Nat. Commun.* **2021**, *12*, 7034.
- (23) Went, C. M.; Wong, J.; Jahelka, P. R.; Kelzenberg, M.; Biswas, S.; Hunt, M. S.; Carbone, A.; Atwater, H. A. A New Metal Transfer Process for van Der Waals Contacts to Vertical Schottky-Junction Transition Metal Dichalcogenide Photovoltaics. *Sci. Adv.* **2019**, *5* (12), 1–8.
- (24) McVay, E.; Zubair, A.; Lin, Y.; Nourbakhsh, A.; Palacios, T. Impact of Al₂O₃ Passivation on the Photovoltaic Performance of Vertical WSe₂ Schottky Junction Solar Cells. *ACS Appl. Mater. Interfaces* **2020**, *12* (52), 57987–57995.
- (25) Hu, Z.; Lin, D.; Lynch, J.; Xu, K.; Jariwala, D. How Good Can 2D Excitonic Solar Cells Be? *Device* **2023**, *1* (1), 100003.
- (26) Hu, Z.; Wang, S.; Lynch, J.; Jariwala, D. Tandem Photovoltaics from 2D Transition Metal Dichalcogenides on Silicon. *ACS Photonics* **2024**, *11*, 4616.
- (27) Munkhbat, B.; Baranov, D. G.; Stührenberg, M.; Wersäll, M.; Bisht, A.; Shegai, T. Self-Hybridized Exciton–Polaritons in Multilayers of Transition Metal Dichalcogenides for Efficient Light Absorption. *ACS Photonics* **2019**, *6* (1), 139–147.
- (28) Wang, S.; Yan, D.; Ibarra Michel, J.; Corletto, A.; Wibowo, A. A.; Balendhran, S.; Lee, H. Y.; Byun, S.; Kim, S.; Crozier, K. B.; Sherrell, P. C.; Macdonald, D.; Bullock, J. Improved Efficiency in WSe₂ Solar Cells Using Amorphous InOx Heterocontacts. *ACS Nano* **2024**, *18* (36), 25046–25052.
- (29) Pettersson, L. A. A.; Roman, L. S.; Inganäs, O. Modeling Photocurrent Action Spectra of Photovoltaic Devices Based on Organic Thin Films. *J. Appl. Phys.* **1999**, *86* (1), 487–496.
- (30) Georgiou, K.; Jayaprakash, R.; Othonos, A.; Lidzey, D. G. Ultralong-Range Polariton-Assisted Energy Transfer in Organic Microcavities. *Angew. Chem.* **2021**, *133* (30), 16797–16803.
- (31) Wang, M.; Hertzog, M.; Börjesson, K. Polariton-Assisted Excitation Energy Channeling in Organic Heterojunctions. *Nat. Commun.* **2021**, *12* (1), 1874.
- (32) Kats, M. A.; Blanchard, R.; Genevet, P.; Capasso, F. Nanometre Optical Coatings Based on Strong Interference Effects in Highly Absorbing Media. *Nat. Mater.* **2013**, *12* (1), 20–24.
- (33) Limonov, M. F.; Rybin, M. V.; Poddubny, A. N.; Kivshar, Y. S. Fano Resonances in Photonics. *Nat. Photonics* **2017**, *11* (9), 543–554.
- (34) Pedersen, T. G.; Latini, S.; Thygesen, K. S.; Mera, H.; Nikolic, B. K. Exciton Ionization in Multilayer Transition-Metal Dichalcogenides. *New J. Phys.* **2016**, *18*, 073043.
- (35) Shockley, W.; Queisser, H. J. Detailed Balance Limit of Efficiency of P-n Junction Solar Cells. *J. Appl. Phys.* **1961**, *32* (3), 510–519.
- (36) Rühle, S. Tabulated Values of the Shockley-Queisser Limit for Single Junction Solar Cells. *Sol. Energy* **2016**, *130*, 139–147.
- (37) Wi, S.; Kim, H.; Chen, M.; Nam, H.; Guo, L. J.; Meyhofer, E.; Liang, X. Enhancement of Photovoltaic Response in Multilayer MoS₂ Induced by Plasma Doping. *ACS Nano* **2014**, *8* (5), 5270–5281.
- (38) Wong, J.; Jariwala, D.; Tagliabue, G.; Tat, K.; Davoyan, A. R.; Sherrott, M. C.; Atwater, H. A. High Photovoltaic Quantum Efficiency in Ultrathin van Der Waals Heterostructures. *ACS Nano* **2017**, *11* (7), 7230–7240.
- (39) Wang, H.; Wang, W.; Zhong, Y.; Li, D.; Li, Z.; Xu, X.; Song, X.; Chen, Y.; Huang, P.; Mei, A.; Han, H.; Zhai, T.; Zhou, X. Approaching the External Quantum Efficiency Limit in 2D Photovoltaic Devices. *Adv. Mater.* **2022**, *34*, 2206122.
- (40) Akama, T.; Okita, W.; Nagai, R.; Li, C.; Kaneko, T.; Kato, T. Schottky Solar Cell Using Few-Layered Transition Metal Dichalcogenides toward Large-Scale Fabrication of Semitransparent and Flexible Power Generator. *Sci. Rep.* **2017**, *7*, 11967.
- (41) Nassiri Nazif, K.; Kumar, A.; Hong, J.; Lee, N.; Islam, R.; McClellan, C. J.; Karni, O.; Van De Groep, J.; Heinz, T. F.; Pop, E.; Brongersma, M. L.; Saraswat, K. C. High-Performance p-n Junction Transition Metal Dichalcogenide Photovoltaic Cells Enabled by MoOx Doping and Passivation. *Nano Lett.* **2021**, *21* (8), 3443–3450.
- (42) Green, M. A.; Dunlop, E. D.; Yoshita, M.; Kopicakakis, N.; Bothe, K.; Siefert, G.; Hao, X.; Jiang, J. Y. Solar Cell Efficiency Tables (Version 65). *Prog. Photovoltaics Res. Appl.* **2024**, *33*, 3–15.
- (43) Ding, C.; Wang, D.; Liu, D.; Li, H.; Li, Y.; Hayase, S.; Sogabe, T.; Masuda, T.; Zhou, Y.; Yao, Y.; Zou, Z.; Wang, R.; Shen, Q. Over 15% Efficiency PbS Quantum-Dot Solar Cells by Synergistic Effects of Three Interface Engineering: Reducing Nonradiative Recombination and Balancing Charge Carrier Extraction. *Adv. Energy Mater.* **2022**, *12* (35), 2201676.